ACCOUNTS
of chemical research

Bonding with Parallel Spins: High-Spin Clusters of Monovalent Metal Atoms

DAVID DANOVICH AND SASON SHAIK*

Institute of Chemistry and the Lise-Meitner-Minerva Center for Computational Quantum Chemistry, The Hebrew University of Jerusalem, 91904 Jerusalem, Israel

RECEIVED ON MAY 24, 2013

CONSPECTUS

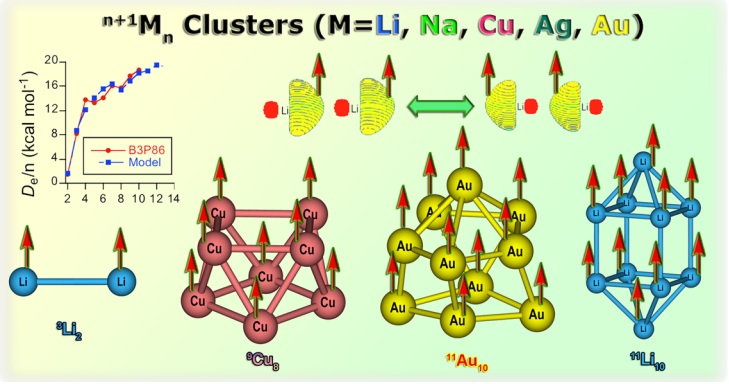

Bonding is a glue of chemical matter and is also a useful concept for designing new molecules. Despite the fact that electron pairing remains the bonding mechanism in the great majority of molecules, in the past few decades scientists have had a growing interest in discovering novel bonding motifs. As this Account shows, monovalent metallic atoms having exclusively parallel spins, such as $^{11}Li_{10}$, $^{11}Au_{10}$, and $^{11}Cu_{10}$, can nevertheless form strongly bound clusters, without having even one traditional bond due to electron pairing. These clusters, which also can be made chiral, have high magnetic moments. We refer to this type as no-pair ferromagnetic (NPFM) bonding, which characterizes the $^{n+1}M_n$ clusters, which were all predicted by theoretical computations. The small NPFM alkali clusters that have been "synthesized" to date, using cold-atom techniques, support the computational predictions.

In this Account, we describe the origins of NPFM bonding using a valence bond (VB) analysis, which shows that this bonding motif arises from bound triplet electron pairs that spread over all the close neighbors of a given atom in the cluster. The bound triplet pair owes its stabilization to the resonance energy provided by the mixing of the local ionic configurations, $[^3M(\uparrow\uparrow)^-]M^+$ and $M^+[^3M(\uparrow\uparrow)^-]$, and the various excited covalent configurations (involving p_z and d_{z^2} atomic orbitals) into the repulsive covalent structure $^3(M\uparrow\uparrow M)$ with the s^1s^1 electronic configuration. The NPFM bond of the bound triplet is described by a resonating wave function with "in−out" and "out−in" pointing hybrids. The VB model accounts for the tendency of NPFM clusters to assume polyhedral shapes with rather high symmetry. In addition, this model explains the very steep rise of the bonding energy per atom (D_e/n), which starts out small in the $^3M_2$ dimer (<1 kcal/mol) and reaches 12−19 kcal/mol for clusters with 10 atoms. The model further predicts that usage of heteroatomic clusters should increase the bonding energy of an NPFM cluster.

These NPFM clusters are excited state species. We suggest here stabilizing these states and making them accessible, for example, by using magnetic fields, or a combination of magnetic and electric fields. The advent of NPFM clusters offers new horizons in chemistry and enriches the scope of chemical bonding. These prospects form a strong incentive to investigate the origins of the bound triplet pairs and further chart the territory of NPFM clusters, for example, in clusters of Be, Mg, or Zn, possibly in clusters of their monosubstituted species, and the group III metalloids, such as B, Al, as well as in transition metals such as Sc.

1. Introduction

The chemical bond is the key element with which chemists can design and comprehend the chemical universe. The most common bond is based on electron pairing between atoms or fragments, thus forming an infinite number of molecules that are linked by these bonds. However, even electrons that have parallel spins and no electron pairing can lead to bonding. This is illustrated in the clusters in

Published on the Web 08/13/2013 www.pubs.acs.org/accounts
10.1021/ar4001422

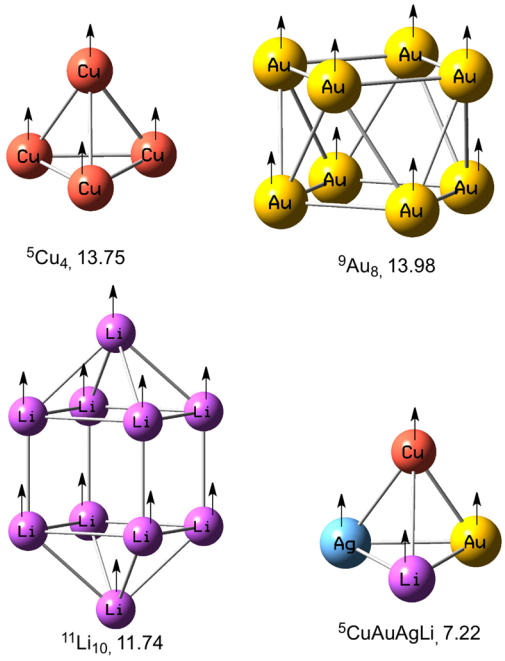

FIGURE 1. Examples of symmetric NPFM clusters[1] and a chiral one.[2] The superscript is the spin multiplicity. The arrows highlight the parallel electron spins. Underneath the structures are bond dissociation energies (kcal/mol) per single atom.

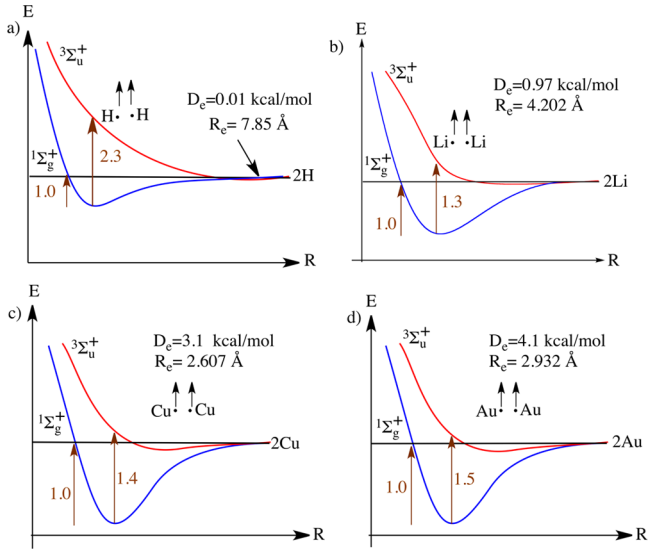

FIGURE 2. Singlet (blue) and triplet (red) energy curves for the ground ($^1\Sigma_g^+$) and the ferromagnetic ($^3\Sigma_u^+$) states of (a) H_2, (b) Li_2, (c) Cu_2, and (d) Au_2. D_e and R_e are, respectively, the computed[1a,2,3a,d,4d] bond energy and equilibrium distance for $^3\Sigma_u^+$. The steepness of the triplet repulsion is indicated by the ratio of the two brown arrows extending from the ground state minimum.

Figure 1, which were predicted in Jerusalem.[1] The first three are symmetric polyhedra, while the fourth is chiral,[2] and all have substantial bond energies even though their electrons are ferromagnetically coupled. Thus, a ferromagnetic arrangement of the valence electrons can lead to polyatomic clusters with high magnetic moments and chirality. Our group investigated the nature of this unusual bonding by means of valence bond (VB) theory and referred to it as no-pair ferromagnetic (NPFM) bonding to emphasize its essential feature. The NPFM bond is the topic of this Account.[1−3]

2. Background

Theory has played a key role in the discovery of this bonding motif. Pioneering studies by Kutzelnigg et al.,[4a] Konowalow,[4b] and Kaldor[4c] predicted that the $^3\Sigma_u^+$ state of $^3Li_2$, which has two parallel spins, should be weakly bonded by ≤1 kcal/mol, which is unlike the $^3H_2$ state,[4d] wherein the depth of the minimum is ∼100 times smaller. As shown in Figure 2a, the $^3\Sigma_u^+$ state H↑↑H has steeply rising repulsion energy. This case should be contrasted with Li↑↑Li, which is shown in Figure 2b to be weakly bonded (D_e = 0.97 kcal/mol[2]), and with Cu↑↑Cu and Au↑↑Au in Figure 2c,d where $^3\Sigma_u^+$ has even stronger bonding. In Figure 2b−d, the triplet repulsion is compensated by an attractive interaction, which we shall shortly discuss.

McAdon and Goddard[5] pointed out in 1987 that this attractive component becomes substantial in $^9M_8$ (M = Li, Cu, Ag, or Au) ferromagnetic rings. In 1993, Gukhovtsev and Schleyer[6] studied Li_2−Li_6 clusters and showed that the high-spin states have optimum geometries with high symmetry and substantial binding energies. They coined the term "no-pair bonding". In 1999, with the advent of efficient VB methods, our group has begun to analyze the bonding mechanism in $^3Li_2$,[3a] and using the VB information, we predicted the trends in the larger clusters and modeled systematically the clusters of the monovalent atoms, Li, Na, K, Cu, Ag, and Au.[1−3] This fascinating chemical bonding mechanism will be analyzed here.

Before proceeding, we note that no-pair alkali clusters have been "synthesized" and spectroscopically probed.[7,8] Helium-nanodroplet isolation involves selective deposition of the highest-spin clusters.[7a] Other techniques use magneto-optical traps of cold atoms.[7d] Much data exist today on the $^3\Sigma_u^+$ states of dimers of alkali atoms and copper,[7a,b,d,8] as well as on some trimer species, $^4Li_3$, $^4Na_3$, and $^4K_3$, that have three parallel spins.[7a,c] Furthermore, the quest for magnetic molecular systems is an active research area in bioinorganic chemistry, nanomedicine, catalysis, and surface science.[9,10] Thus, understanding the nature of the NPFM bond becomes even more essential.

The Account starts by describing our studies and VB modeling of the bonding in NPFM clusters of lithium and other alkali metals.[1−3] It then continues with the coinage metals and heteroatomic and chiral clusters and ends with generalizations about this type of bonding.

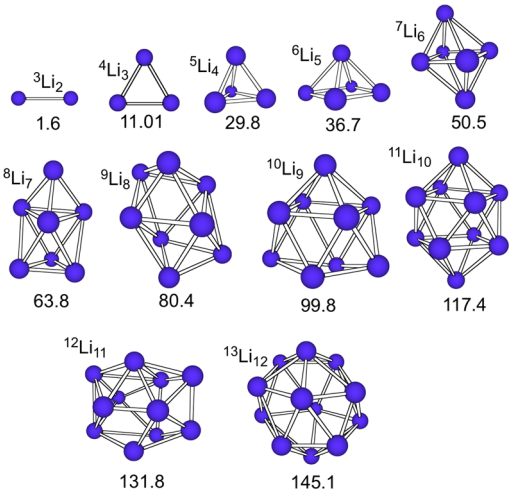

FIGURE 3. NPFM $^{n+1}Li_n$ clusters and their bonding energies (kcal/mol) calculated with B3P86.[2] Reproduced with permission from Figure 5 of ref 1b. Copyright 2002 American Chemical Society.

3. NPFM Bonding in $^{n+1}Li_n$ ($n = 2-10$)

Figure 3 shows the density functional theory (DFT) calculations of $^{n+1}Li_n$ clusters.[1b,3a] It is seen that the bonding energy climbs fast and reaches ~12 kcal/mol per Li atom.

To highlight the structural features of these NPFM clusters, we display in Figure 4 examples of $^{5}Li_4$ and $^{7}Li_6$ vis-à-vis the singlet ground state clusters.[1b,2] It is seen that while $^{5}Li_4$ is a symmetric tetrahedron, the ground state $^{1}Li_4$ is a planar rhombus. Similarly, $^{7}Li_6$ is a distorted octahedron, while $^{1}Li_6$ has two closely lying structures,[11] the most stable one being an antiprism with bond distances that differ by ~1 Å.[2]

The results for clusters up to $^{7}Li_6$ were verified by coupled-cluster theory with singles, doubles, and perturbational triples (CCSD(T)) by us[3a] and by Monari et al.[12] (see Supporting Information, Table S2). Nevertheless, we emphasize here that the bonding energies in Figure 3 do not represent dispersion-binding energies,[13] but arise from orbital mixing effects. Others reached a similar conclusion for $^{5}Li_4$ and $^{4}Li_3$ ($^{4}A'_2$).[12a,14] We shall now proceed to comprehend the intriguing rise in the bonding energy of the NPFM clusters $^{n+1}Li_n$ and their unique geometric features.[1,3]

4. Origins of NPFM Bonding in $^{n+1}Li_n$ Clusters

4.1. The $^{3}\Sigma_u^+$ State of $^{3}Li_2$. As was shown in 1999,[3a] *ab initio* calculations of the bonding energy in $^{3}Li_2$ require a method that involves static and dynamic correlations, like CCSD(T) or multistructure VB methods.[15] The chosen level was the breathing-orbital VB (BOVB) method that involves both static and dynamic electron correlations.[16] The results are described in Figure 5. Figure 5a shows the VB structures that can be generated by distributing the two triplet electrons

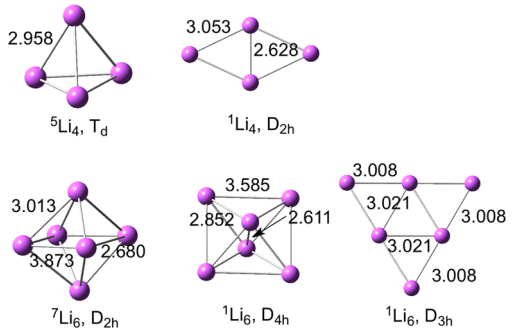

FIGURE 4. The structures and key bond lengths (Å) of the NPFM clusters $^{5}Li_4$ and $^{7}Li_6$ vis-à-vis their ground state clusters $^{1}Li_4$ and $^{1}Li_6$,[2] calculated with B3P86.[1b]

in the valence orbitals. The fundamental configuration is $^{3}\Phi_{ss}$, which accommodates the electrons in the 2s orbitals of the lithium atoms. The structure labeled as $^{3}\Phi_{sz}$(ion) is a triplet charge-transfer (^{3}CT) structure, wherein one electron is transferred from the 2s orbital of one Li to the $2p_z$ orbital of the second; there are two such structures. Finally, $^{3}\Phi_{zz}$(cov) and $^{3}\Phi_{xx(yy)}$(cov) are covalent structures, where the electrons are excited to the 2p orbitals.

Figure 5b shows the energy curves of various state-wave functions. Starting from the left, the first one shows the energy of $^{3}\Phi_{ss}$ plotted along the Li···Li distance. It is seen that this structure is repulsive, much like $^{3}H_2$ (Figure 2a). The second plot shows that adding $^{3}\Phi_{sz}$(ion) to $^{3}\Phi_{ss}$ results already in incipient bonding. Adding the other structures in the subsequent plots deepens the energy well to its final BOVB values, which are $D_e = 0.639$ with a cc-pVDZ basis set and 0.888 kcal/mol for cc-pCVTZ;[3a] the CCSD values[3a] for the two basis sets are $D_e = 0.738$ and 0.902 kcal/mol. The agreement of VB with the coupled cluster method is satisfactory. Similarly, the BOVB results for $^{3}Na_2$ (0.40 kcal/mol) and $^{3}K_2$ (0.46 kcal/mol)[2] are in accord with the CCSD(T) results and experimental trends.[14]

The final VB wave function for $^{3}Li_2$ is

$$^{3}\Psi(^{3}\Sigma) = 0.909\,^{3}\Phi_{ss} + 0.029\,^{3}\Phi_{sz}(\text{ion}) + 0.027\,^{3}\Phi_{zz}(\text{cov}) + 0.003\,^{3}\Phi_{xx(yy)}(\text{cov}) \qquad (1)$$

It is seen that the NPFM state of $^{3}Li_2$ is dominated by the fundamental structure but exhibits significant mixing of the ^{3}CT structure and the excited covalent structure $^{3}\Phi_{zz}$(cov). The effect of the off-axis π-type $^{3}\Phi_{xx(yy)}$(cov) structures is smaller.

4.2. Orbital Cartoons for the NPFM Bonding of the $^{3}\Sigma_u^+$ State of $^{3}Li_2$. No doubt, all the calculations show the importance of s–p mixing for bonding.[1,12a,14] However,

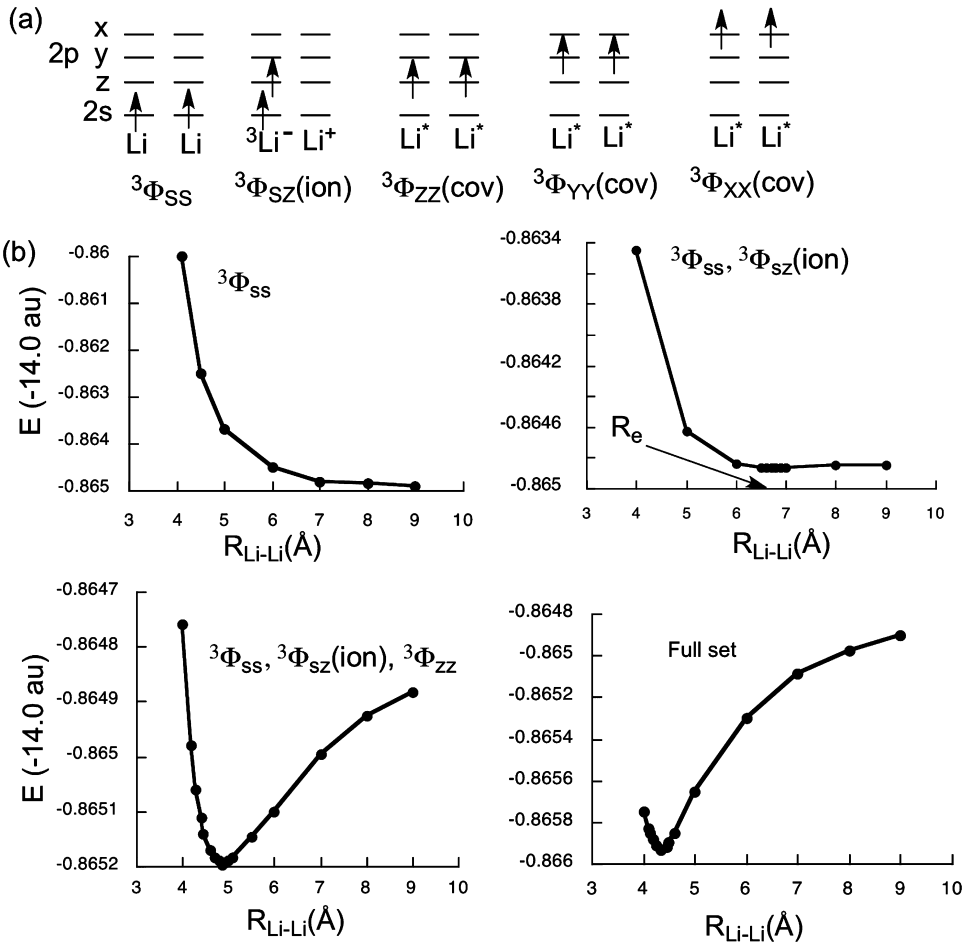

FIGURE 5. NPFM bonding in $^3Li_2$. (a) Fundamental ($^3\Phi_{ss}$) and excited VB structures ($^3\Phi_{sz}$(ion), $^3\Phi_{zz}$(cov), and $^3\Phi_{xx(yy)}$(cov); the Li–Li axis is *z*). (b) BOVB computed[2] energy variation along the Li–Li distance for various VB wave functions. Reproduced with permission from Figure 3 in ref 3a. Copyright 1999 American Chemical Society.

does the above wave function simply reflect standard s–p hybridization effects? To see the kind of hybridization, we derived orbitals, which represent the mixed VB wave function, eq 1.[1b] Figure 6 shows the resulting orbital cartoons for various stages of the NPFM-bond wave function for the $^3\Sigma_u^+$ state.[2]

Figure 6a depicts the orbitals for the repulsive fundamental VB structure $^3\Phi_{ss}$, which are the 2s orbitals of the two Li atoms, having parallel-spin electrons. By adding $^3\Phi_{zz}$(cov) with some coefficient and transforming the orbitals,[1b,2,3a] we obtain the two resonating VB structures in Figure 6b wherein the 2s and $2p_z$ AOs are hybridized or mixed. It is seen that in each structure in Figure 6b, the triplet electrons occupy an "in–out" or an "out–in" pair of hybrids. This hybridization mode decreases the orbital overlap for the electron pair, thus mitigating the triplet repulsion. Simultaneously, the resonating state enjoys some resonance-energy stabilization. Finally, adding the CT structures, $^3\Phi_{sz}$(ion), to the "in–out" ⟷ "out–in" resonating wave function causes

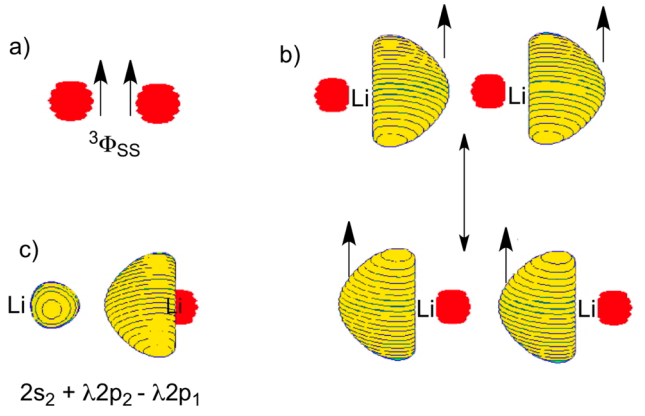

FIGURE 6. Orbital cartoons for the $^3\Sigma_u^+$ state in eq 1: (a) The 2s orbitals in $^3\Phi_{ss}$. (b) The hybrids for the resonating wave function of $^3\Phi_{ss}$ and $^3\Phi_{zz}$(cov). (c) The orbital on the right-hand Li atom after adding also the $^3\Phi_{sz}$(ion) structures. Reproduced with permission from Scheme 3 in ref 1b. Copyright 2002 American Chemical Society.

each hybrid to develop a small delocalization tail on the other atom as shown in Figure 6c. Much like in generalized-VB

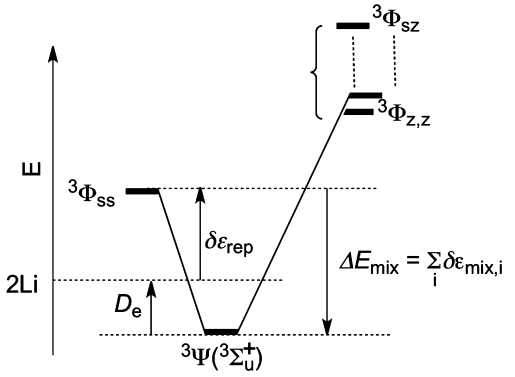

FIGURE 7. VB-mixing diagram describing the bonding in $^3Li_2$ as a result of mixing of the excited VB structures into the fundamental structure. $\delta\varepsilon_{rep}$ is the Pauli repulsion energy of $^3\Phi_{ss}$. ΔE_{mix} is the mixing energy due to the various excited configurations.

theory,[17] the delocalization tails provide additional bonding to the wave function. Thus, each VB structure plays a clear physical role in shaping the NPFM bonding of Li_2 in the $^3\Sigma_u^+$ state: the $^3\Phi_{zz}$(cov) structure lowers the Pauli repulsion of the fundamental structure and contributes some resonance energy, while $^3\Phi_{sz}$(ion) adds covalent−ionic resonance energy[15] that further binds the triplet pair. An alternative representation of NPFM-bonding was described by McAdon and Goddard,[5] using interstitial (1e-bond) orbitals, which incorporate to some extent the energetic effects of the mixing discussed above.[1b,3a]

4.3. VB Mixing Diagram for $^3Li_2$. The above effects can be cast in terms of the VB mixing diagram in Figure 7. It is seen that $^3\Phi_{ss}$ suffers from Pauli repulsion ($\delta\varepsilon_{rep}$) relative to the two separate Li atoms. As the excited structures mix with the fundamental structure, a mixing energy, ΔE_{mix}, stabilizes $^3\Phi_{ss}$ and confers a small bonding energy, D_e.

4.4. VB Modeling of $^{n+1}Li_n$ Patterns. The results of $^3Li_2$ can be used to construct a useful model for predicting the expected trends in larger clusters, $^{n+1}Li_n$. Consider a Li atom, numbered *j* in Scheme 1a and having a coordination number C_j. In the fundamental structure, each linkage of Li(*j*) is described by the VB structure of the dimer, $^3\Phi_{ss}$, which possesses parallel spins having a Pauli repulsion, $\delta\varepsilon_{rep}$, and is stabilized by mixing with the excited ^{3}CT and covalent VB structures. The number of these excited VB structures depends on the number of orbitals that each Li atom utilizes for distributing the triplet pair. If we exclude the 2p orbital that maintains π-type overlap with others, we are left with the 2s orbital and two tangential 2p orbitals. Hence, the number of orbitals (N_{ao}) that each atom contributes to the cluster is three as indicated in Scheme 1a ($N_{ao} = 2$ for $^3Li_2$). As such, each Li···Li linkage in the cluster will form a NPFM bond described by a wave function involving the fundamental

SCHEME 1. (a) A j^{th} Li Atom in the Cluster and Its Repulsive Triplet Pairs with Its Close Neighbors[a] and (b) A VB Mixing Diagram of $^{n+1}\Phi_{s(1)s(2)...s(j)...s(n)}$ with the Stack of the Excited VB Structures $\{^{n+1}\Phi_{ex}(i)\}$

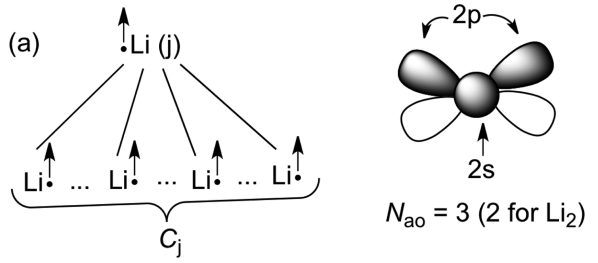

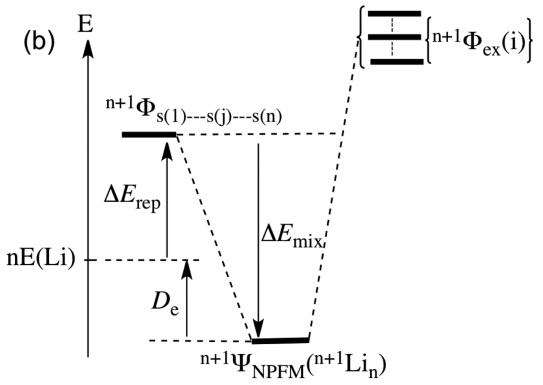

[a] C_j is the corresponding coordination number. N_{ao} is the number of orbitals each atom uses for distributing the triplet pair.

structure mixed with the corresponding excited ^{3}CT and cova lent structures. As shown in Scheme 1b, the bonding energy, D_e, is the balance between the Pauli repulsion, ΔE_{rep}, of all the Li atoms with their close neighbors, and the total mixing energy, ΔE_{mix}, due to all the excited VB structures that arise by distributing all the triplet pairs in the available orbitals of the close neighboring Li···Li linkages. This generates NPFM bonds that are delocalized over the entire close neighboring Li···Li linkages.

The modeling is then straightforward. We first count all the close-neighbor repulsion terms in the fundamental structure of the cluster, $^{n+1}\Phi_{s(1)s(2)...s(j)...s(n)}$, and all the excited structures $\{^{n+1}\Phi_{ex}(i)\}$ that contribute mixing terms. We then assign to these terms quantitative values, taken from the dimer,[1b,3a] $\delta\varepsilon_{rep} = 1.504$ kcal/mol and $\Delta E_{mix} = -2.145$ kcal/mol. Since primarily three excited VB structures contribute to the ΔE_{mix} term in the dimer, for simplification we attribute to each one an average mixing term of $\delta\varepsilon_{mix} = -0.714$ kcal/mol.

The total Pauli repulsion in the fundamental VB structure is a sum of the pair-repulsion terms of the close neighbors in the cluster. This repulsion is minimized when all the terms are identical.[1b,2,3a] The resulting expression is eq 2:

$$\Delta E_{rep} = 0.5\delta\varepsilon_{rep}\sum_j C_j = 0.5\delta\varepsilon_{rep}C_{tot} \qquad (2)$$

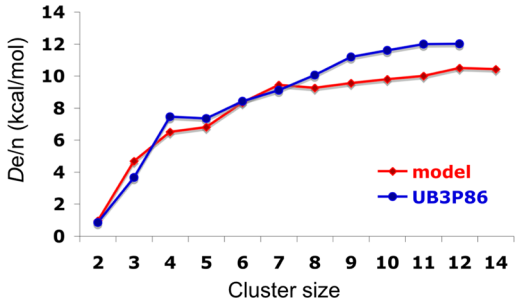

FIGURE 8. D_e/n values (kcal/mol) calculated by B3P86 (blue)[2] and the VB model, eq 4 (red), plotted against the $^{n+1}Li_n$ cluster size, n.[1]

Thus, the repulsive energy of the fundamental structure is the product of fundamental close-neighbor repulsion ($\delta\varepsilon_{rep}$) energy times the total coordination number, C_{tot}, of all atoms in the cluster; the factor 0.5 avoids double counting of the terms. Since the repulsion is minimized when all the terms are identical, *it follows that the NPFM clusters will have a propensity for structures with uniform atom−atom distances*.

In turn, the VB mixing term, ΔE_{mix}, is a product of the individual mixing term, $\delta\varepsilon_{mix}$, times the number of excited VB structures, as shown by eq 3, where N_{ao} is the number of participating valence orbitals (Scheme 1a):

$$\Delta E_{mix} = [0.5(N_{ao}^2 - 1)C_{tot} + N_{ao}]\delta\varepsilon_{mix} \quad (3)$$

The bond energy is the negatively signed balance between the mixing and repulsive terms, becoming

$$D_e(^{n+1}Li_n) = -[0.5(N_{ao}^2 - 1)C_{tot} + N_{ao}]\delta\varepsilon_{mix} - 0.5C_{tot}\delta\varepsilon_{rep} \quad (4)$$

Furthermore, for an infinite cluster, the bond energy per atom, D_e/n, is simply

$$\frac{D_e(^{n+1}Li_n)}{n} \approx -4C_{av}\delta\varepsilon_{mix} - 0.5C_{av}\delta\varepsilon_{rep} \quad (n \rightarrow \text{infinity}) \quad (5)$$

C_{av} is the average coordination number of an atom in the cluster. Equations 4 and 5 together predict in principle that NPFM clusters will tend to assume structures having optimal coordination numbers, which maximize the mixing terms that stabilize the NPFM bonds of a given atom with its close neighbors. The mixing terms prefer shorter distances, and hence, the interplay of repulsion, which prefers uniform bond lengths, with mixing, will tend to produce clusters with nonuniform distances.

Figure 8 plots the bonding energy per atom, D_e/n, against the cluster size. The blue curve corresponds to the DFT

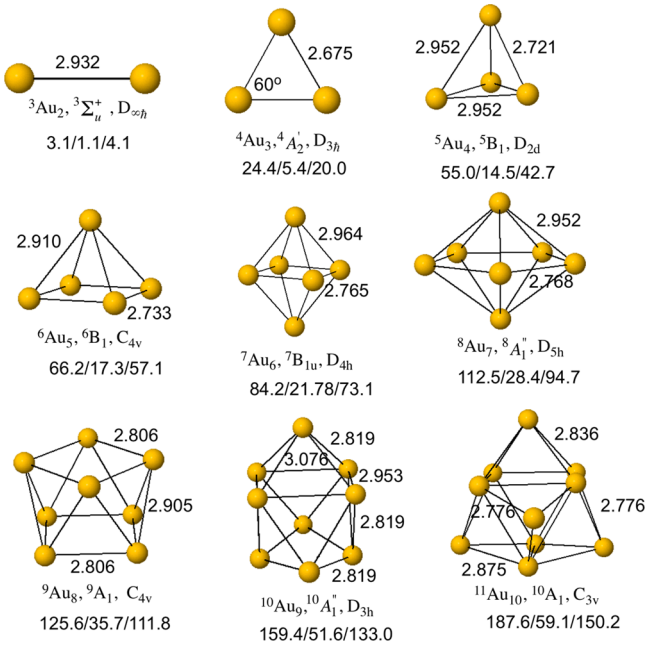

FIGURE 9. B3P86 optimized structures,[2] their point groups, and state assignments for the most stable NPFM clusters, $^{n+1}M_n$, of coinage metals. Bond lengths (Å) are shown for $^{n+1}Au_n$. The D_e values (kcal/mol) beneath the structures are listed in the order Cu/Ag/Au. Adapted with permission from ref 1a. Copyright 2010 American Chemical Society.

results, while the red one traces the VB predicted values (eq 4). Thus, the VB curve reproduces the jump in D_e/n on going from $n = 2$ to $n = 4$ (C_{av} is quadrupled), and then the steep rise and the convergence of the bond energy per atom near $n = 10$. The converged VB value is 10.5 vs ~12 kcal/mol for the DFT calculations.[1b] It is apparent that the VB model captures the computational trends, including the propensity of NPFM clusters for symmetric objects, based on the minimum Pauli repulsion argument.

The same treatment can be applied to all NPFM clusters of the other alkali metals. The $^{n+1}Na_n$ clusters have already been investigated by VB[2] and DFT,[3b] and it was demonstrated that the bonding energies are much lower than in the corresponding $^{n+1}Li_n$ clusters due to the higher 4s−4p orbital-energy gap in Na and the longer Na···Na distances. These two factors raise the energy of the excited VB structures and lower the mixing term and thereby reduce D_e/n drastically.

5. NPFM Bonding in Coinage Metal Clusters[1a,3c]

Coinage metals possess valence configurations $nd^{10}(n+1)s^1$ and are analogous to the alkali metals. However, the d-electrons and the relativistic effects[3d] are expected to make the NPFM clusters of the coinage metals stickier than the corresponding alkali cluster.

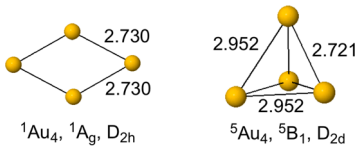

FIGURE 10. B3P86 optimized structures[2] and key bond lengths (Å) of the NPFM cluster $^5Au_4$ and the corresponding ground state $^1Au_4$.[1a]

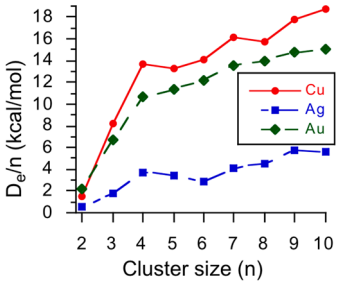

FIGURE 11. Plots of D_e/n (kcal/mol) as a function of cluster size for the $^{n+1}M_n$ clusters of the coinage metals. Reproduced with permission from ref 1a. Copyright 2010 American Chemical Society.

5.1. Structure and Bonding of Coinage Metal NPFM Clusters. Figure 9 shows that like in the Li clusters, here too the most stable NPFM coinage-metal structures are three-dimensional starting already with $^5M_4$.[1a,3c,12b]

Figure 10 shows, side by side, the structures of $^5Au_4$ and the ground state $^1Au_4$. Note that the bond lengths in $^5Au_4$ are not much longer than those of the $^1Au_4$ ground state despite the fact that the NPFM cluster is bonded without a single electron pair.

The D_e values in Figure 9 exhibit a familiar trend to the lithium clusters, showing that NPFM bonding, which starts weak in the dimer, reaches as much as 187.6 kcal/mol for the $^{11}Cu_{10}$ cluster. The D_e/n quantity, which is plotted in Figure 11, is seen to increase steeply by about 10−15 times as the cluster grows, reaching 19 kcal/mol for copper and 15−16 kcal/mol for gold. The silver clusters are rather weakly bonded, and the D_e/n value converges to less than 6 kcal/mol for $^{11}Ag_{10}$.

6. VB Modeling of NPFM Bonding in Coinage Metal Clusters

Figure 12 depicts a few excited VB structures and the VB-mixing diagram for the $^3M_2$ species. As shown in Figure 12a, the fundamental structure is the covalent $^3\Phi_{ss}$ with two valence electrons having parallel spins in the $(n+1)$s orbitals of the two atoms. The excited structures involve singly occupied $(n+1)p_z$ and nd_{z^2} orbitals. There are ^{3}CT structures, like $^3\Phi_{sz^2}$, which involves electron transfer from nd_{z^2} of one metal to $(n+1)$s of the second, or $^3\Phi_{sz}$, which involves an

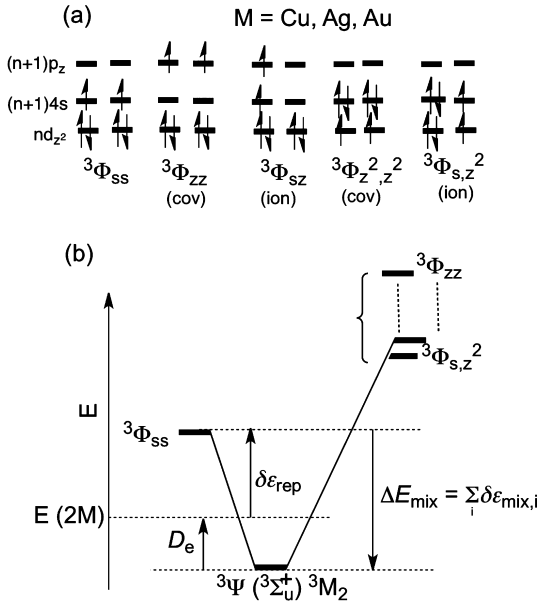

FIGURE 12. (a) Some VB configurations that contribute to NPFM-bonding in the no-pair dimers, $^3M_2(^3\Sigma_u^+)$, of coinage metals. (b) The corresponding VB-mixing diagram. Reproduced with permission from ref 1a. Copyright 2010 American Chemical Society.

electron transfer from $(n+1)$s of one atom to $(n+1)p_z$ of the second. In addition, there are excited covalent structures, wherein the two valence electrons occupy the $(n+1)p_z$ orbitals of both atoms, as in $^3\Phi_{zz}$, or the nd_{z^2} orbitals, as in $^3\Phi_{z^2z^2}$. Thus, having more excited VB structures, the coinage metals can sustain stronger NPFM bonding compared with the alkali metals in the same period.

The fundamental $^3\Phi_{ss}$ configuration is repulsive, and the repulsive term, $\delta\varepsilon_{rep}$, in Figure 12b arises from the triplet electrons as well as from the Pauli repulsions of the d^{10}−d^{10} shells. The NPFM bonding is brought about by the mixing of the excited configurations, each of which contributes a $\delta\varepsilon_{mix,i}$ stabilization. Thus, the net NPFM bonding will reflect a balance between the repulsive interactions in the fundamental structure and the sum of the mixing terms due to all the excited structures. As we move to larger clusters, there will always be one fundamental structure, $^{n+1}\Phi_{s(1)s(2)...s(n)}$, with repulsive interactions of the parallel spins in the ns orbitals and d^{10}−d^{10} shells on neighboring atoms. But at the same time, the number of excited VB structures available to each metal in the cluster will increase steeply and bring about NPFM bonding in $^{n+1}M_n$.

As shown for $^{n+1}Li_n$,[3a] here too D_e can be expressed in an analytical form.[1a,2,3a] Again, we use a uniform repulsion term ($\delta\varepsilon_{rep}$) for close neighbors, such that the total repulsion is the product of $\delta\varepsilon_{rep}$ by the total coordination number of all the atoms in the cluster, C_{tot}. In addition, assuming that the

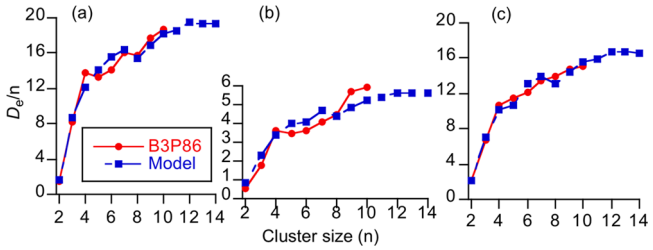

FIGURE 13. Plots of B3P86 calculated[2] (red) and VB-modeled (blue) D_e/n values (kcal/mol) as function of cluster size, for $^{n+1}M_n$ clusters of (a) M = Cu, (b) M = Ag, and (c) M = Au. Reproduced with permission from ref 1a. Copyright 2010 American Chemical Society.

various excited configurations each contribute an identical close-neighbor mixing term, $\delta\varepsilon_{mix}$, allows us to evaluate the total mixing term for any cluster size by counting the number of excited CT and covalent VB structures that a given atom shares with its close neighbors. We use only the lowest excitations involving electron shifts from the *n*d AOs to singly occupied (*n*+1)s AOs and from (*n*+1)s to (*n*+1)p. The resulting expression for the NPFM binding energy is eq 6:[1a,2,3c]

$$D_e = -\left[\frac{(N_{ao}{}^2+9)C_{tot}}{2}+N_{ao}\right]\delta\varepsilon_{mix}-\frac{C_{tot}\delta\varepsilon_{rep}}{2} \quad (6)$$

Compared with $^{n+1}Li_n$ (eq 4), here the multiplier of $\delta\varepsilon_{mix}$ is significantly larger,[1a,2] since now there are additional ionic and covalent structures that result from participation of the *n*d orbitals.[12b]

Since a full VB calculation of coinage metals is still tedious, we calculated only the triplet repulsion in s^1s^1, while least-squares fitting the mixing term in eq 6 to the computed D_e/n quantities. To test the fit, we also used least-squares fitting of both the repulsion and mixing terms. Both approaches led to similar results (see Supporting Information document of ref 1a.).

Figure 13 shows plots of the VB modeled and DFT computed D_e/n values for the coinage NPFM clusters vs the cluster size *n*. It is seen that the VB model describes fairly well the entire pattern of NPFM bonding in these three coinage metals, converging to D_e/n values of 19.5 kcal/mol for copper, 16.5 kcal/mol for the gold, and 5 kcal/mol for silver.

It is instructive to consider the trends in $\delta\varepsilon_{rep}$ and $\delta\varepsilon_{mix}$. The VB computed triplet pair repulsion terms, $\delta\varepsilon_{rep}$, change in the order Cu > Au > Ag (14.3, 11.8, and 8.6 kcal/mol). The smaller repulsion of Au versus Cu reflects the relativistic shrinkage[18] of the 6s orbitals of Au, which lowers the $6s^1-6s^1$ repulsion. All these values are much larger than that for Li ($\delta\varepsilon_{rep}$ = 1.504 kcal/mol), since the coinage metals have in addition to s^1-s^1 also $d^{10}-d^{10}$ repulsive terms.

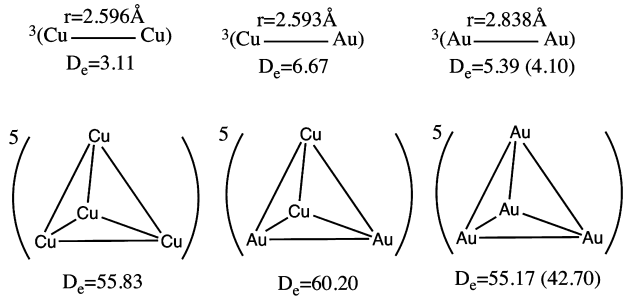

FIGURE 14. Homo- and heteroatomic NPFM clusters and their D_e values (kcal/mol). Values out of parentheses are obtained with a common level.[2]

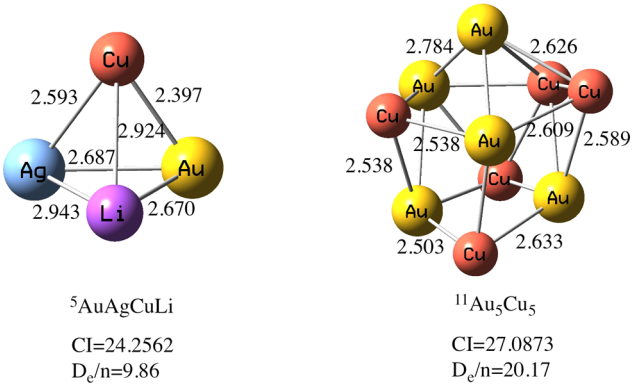

FIGURE 15. Chiral heteroatomic NPFM clusters and their chirality index (CI), D_e/n values (kcal/mol), and bond lengths (Å).

The best-fitted $\delta\varepsilon_{mix}$ terms are −1.3245, −0.6902, and −0.1653 kcal/mol for Cu, Au, and Ag, respectively. These terms vary in an inversely proportional manner to the calculated d−s orbital energy gaps in the atoms;[1a] this trend can in turn be understood using principles outlined by Pyykkö and Desclaux.[18] Thus, Cu is affected by the "$3d^{10}$-contraction", and hence its 3d−4s gap should be smaller than the 4d−5s gap in Ag, while in Au, the 5d−6s gap shrinks compared with Ag by the relativistic shrinkage.

The VB model can be used also to account for a puzzling behavior of the Cu versus Au clusters. Thus, as can be seen from Figure 9, $^3Au_2$ is more strongly bonded than $^3Cu_2$. By contrast, as the cluster grows, the trend is reversed, and the Cu clusters become more strongly bonded. Based on eq 6, as the cluster grows, the number of excited VB structures (given by the square-bracketed terms in front of $\delta\varepsilon_{mix}$) increases much faster than the number of repulsions. Initially, the $^3Cu_2$ dimer, with the larger repulsive term, has a smaller D_e/n compared with $^3Au_2$. However, as the cluster grows, the VB mixing energy starts dominating the trend, and since the elementary mixing term for Cu is significantly larger than the one for Au, the D_e and D_e/n values for the $^{n+1}Cu_n$ clusters become larger than for those the $^{n+1}Au_n$ clusters.

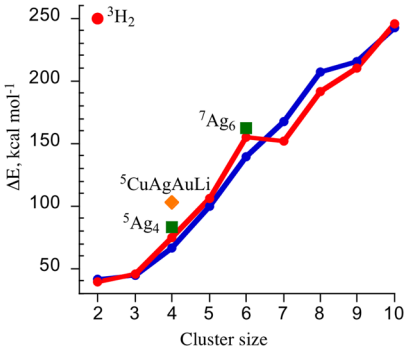

FIGURE 16. B3P86 excitation energies[2] (ΔE, kcal/mol) from the ground to the no-pair states for $^{n+1}Cu_n$ (blue) and $^{n+1}Au_n$ (red) clusters. Data are shown also for $^3H_2$ and $^{n+1}Ag_n$ clusters.

7. Heteroatomic NPFM Clusters

Since ^{3}CT structures contribute to NPFM bonding, it is reasonable to expect that heteroatomic clusters will be even more strongly bound than homoatomic ones. As shown in Figure 14, this is indeed the case for ^{3}(CuAu) and ^{5}(Au_2Cu_2), which are more strongly bound than their corresponding homoatomic clusters, $^3Au_2$, $^3Cu_2$, $^5Cu_4$, and $^5Au_4$. Thus, heteroatomic substitution is a strategy for creating more stable NPFM clusters.

Heteroatomic substitution is also a strategy for making chiral NPFM clusters. Figure 15 shows ^{5}(AuAgCuLi) and ^{11}-(Au_5Cu_5). The chirality[19] of the first cluster is achieved by usage of four different atoms, while in the second it is due to the helical arrangement of the atoms. These examples show that NPFM bonding leads to strongly bound clusters that possess high magnetic moments and chirality.

8. Generalization of NPFM Bonding: Resonating Bound Triplet Pairs

The above discussion shows that the VB modeling captures the essence of the NPFM bonding in the clusters of alkali and coinage metals. The bonding is provided by the resonance energy due to mixing of the local ionic structures, $[^3M(\uparrow\uparrow)^-]M^+$ and $M^+[^3M(\uparrow\uparrow)^-]$, and the various excited covalent structures (involving p_z and d_{z^2} triplet pairs) into the repulsive fundamental covalent structure ^{3}(M↑↑M) with the s^1s^1 electronic structure. *This creates bound triplet electron pairs that are delocalized over all the close neighbors of a given atom in the cluster*.

As we demonstrated for $^{n+1}Li_n$ clusters,[1b,3a] in Figure 6, the VB wave function of the NPFM bond can be represented by a cartoon involving a resonating wave function with hybrid orbitals that assume "in−out" ⇔ "out−in" orientations and delocalization tails.[1b] Thus, if we consider each close neighboring triplet pair as a local NPFM bond, we can regard the electronic structure of a given $^{n+1}M_n$ cluster as *a resonance hybrid of all the local NPFM bonds formed by each atom with its close neighbors*. This delocalization is apparent also from the electron localization function (ELF)[20] analysis of the electron density in $^3Li_2-^7Li_6$,[21] as well as from the interstitial 1e-bond orbitals in the GVB modeling.[5]

9. Prospective

NPFM clusters of monovalent metallic atoms having *exclusively parallel spins* are nevertheless strongly bonded, reaching D_e/n values of 12−19 kcal/mol. The NPFM bonding is conferred upon these clusters by the mixing of local ^{3}CT and excited covalent structures into the repulsive fundamental s^1s^1 structure, thus creating *a parallel-spin system stabilized by resonance energy and delocalized over the entire cluster*. These clusters have polyhedral shapes and high magnetic moments, and they also can be made chiral. It was shown that increasing the bonding energy of these clusters could be achieved by usage of heteroatomic clusters.

The strength of these local NPFM bonds depends on the metal atom and is larger in coinage metals than in the alkali metals due to the involvement of the d^{10} shell in delocalizing the triplet pair.[1a,12b] In each family, the D_e/n is largest for the first-row element (Li, Cu) and weakest for the second row (Na, Ag). A more complete territory of NPFM clusters may be explored in clusters of monosubstituted species of Be, Mg,[22] Zn, etc., of the group III metalloids, like B, Al, and of transition metals like Sc, etc.

The NPFM clusters are excited state species, but as magnetic objects,[23] they may still have potential applications in nanochemistry. An additional potential interest in NPFM clusters is their relationship to Bose−Einstein condensates, and to Fermi "gases" of fermionic isotopes (e.g., ^{6}Li) in magnetic fields.[24] The existence of "synthetic methods" for no-pair dimers and trimers[7,8] gives hope that a stepwise growth of larger clusters may eventually be achieved. The finding of sudden magnetization upon adsorption of organic molecular layers on gold surfaces[10] merits exploration regarding the nascence of magnetic states on the gold surface and their potential relation to NPFM clustering.

Intriguingly, Lange et al.[25] showed recently that in magnetic fields as large as those existing in white dwarfs,[26] even $^3H_2$ becomes bound and accessible as a ground state. As shown in Figure 16, compared with $^3H_2$, the NPFM states described here lie closer to their ground states. This and the high magnetic moments of the larger clusters will require weaker magnetic fields[3e] to become ground states. External electric fields[3c] and heteroatomic substitution may further stabilize the NPFM state. The usage of NPFM clusters may offer new chemical horizons.

Supporting Information. Methodology, VB repulsion and structure counts, benchmarking of DFT vs CCSD(T), Cartesian coordinates, and additional references. This material is available free of charge via the Internet at http://pubs.acs.org.

Note Added after ASAP Publication. This paper was published ASAP on August 13, 2013. A change was made to equation 6 and Figure 15 was replaced. The revised version was reposted on October 16, 2013.

BIOGRAPHICAL INFORMATION

David Danovich is senior research associate at the Hebrew University and a former graduate of Irkutsk State University, Russia. His major interests are in bonding and method developments.

Sason Shaik is currently the Director of the Lise Meitner-Minerva Center at the Hebrew University. His major interests are in developing concepts for bonding and reactivity.

FOOTNOTES

*Phone, +972-2-6585909; fax, +972-2-6584680/6585345; e-mail, sason@yfaat.ch.huji.ac.il.

The authors declare no competing financial interest.

This Account is dedicated to Helmut Schwarz, a geat scientist and a Mentsch, for his 70th Birthday.

REFERENCES

1 (a) Danovich, D.; Shaik, S. Bound Triplet Pairs in the Highest Spin Sates of Coinage Metal Clusters. *J. Chem. Theory Comput.* **2010**, *6*, 1479–1489. (b) de Visser, S. P.; Danovich, D.; Wu, W.; Shaik, S. Ferromagnetic Bonding: Properties of High-Spin Lithium Clusters, $^{n+1}Li_n$ (n = 2−12) Devoid of Electron Pairs. *J. Phys. Chem. A* **2002**, *106*, 4961–4969.

2 Consult the Supporting Information for methodological details, basis sets, and new calculations.

3 (a) Danovich, D.; Wu, W.; Shaik, S. No-Pair Bonding in the High-Spin $^3\Sigma_u^+$ State of Li_2. A Valence Bond Study of Its Origins. *J. Am. Chem. Soc.* **1999**, *121*, 3165–3174. (b) de Visser, S. P.; Danovich, D.; Shaik, S. Ferromagnetic Bonding in High-Spin Alkali Metal Clusters. How Does Sodium Compare to Lithium? *Phys. Chem. Chem. Phys.* **2003**, *5*, 158–164. (c) de Visser, S. P.; Kumar, D.; Danovich, M.; Nevo, N.; Danovich, D.; Sharma, P. K.; Wu, W.; Shaik, S. Ferromagnetic Bonding: High Spin Copper Clusters ($^{n+1}Cu_n$; n = 2−14) Devoid of Electron Pairs but Possessing Strong Bonding. *J. Phys. Chem. A* **2006**, *110*, 8510–8518. (d) Danovich, D.; Filatov, M. No-Pair Bonding in Coinage Metal Dimers. *J. Phys. Chem. A* **2008**, *112*, 12995–13001. (e) Shaik, S.; Danovich, D. A Comment on Paramagnetic Bonding Mechanism in Strong Magnetic Fields. *Comput. Chem. Highlights*, 2012, August 17th Issue.

4 (a) W. Kutzelnigg, W.; Staemler, V.; Gélus, M. Potential Curve of the Lowest Triplet State of Li_2. *Chem. Phys. Lett.* **1972**, *13*, 496–500. (b) Olson, M. L.; Konowalow, D. D. Accurate Potential Energy Curves for the $^3\Sigma_u^+$ and $^3\Sigma_g^+$ States of Li_2. *Chem. Phys.* **1977**, *21*, 393–399. (c) Kaldor, U. Li_2 Ground States by Open-Shell Coupled Cluster Method. *Chem. Phys.* **1990**, *140*, 1–6. (d) $D_e \leq 0.012$ kcal/mol, in Kolos, W.; Wolntewicz, L. Potential-Energy Curves for the $X^1\Sigma_g^+$, $b^3\Sigma_u^+$, and $c^1\Pi_u$ States of the Hydrogen Molecule. *J. Chem. Phys.* **1965**, *43*, 2429–2441.

5 (a) McAdon, M. H.; Goddard, W. A., III Charge Density Waves, and Peierls Distortions in One-Dimensional Metals. I. Hartree-Fock Studies of Cu, Ag, Au, Li, and Na. *J. Chem. Phys.* **1988**, *88*, 277–302. (b) McAdon, M. H.; Goddard, W. A., III Generalized Valence Bond Studies of Metallic Bonding: Naked Clusters and Application to Bulk Metals. *J. Phys. Chem.* **1987**, *91*, 2607–2626. (c) McAdon, M. H.; Goddard, W. A., III Charge Density Waves, Spin Density Waves, and Peierls Distortions in One-Dimensional Metals. 2. Generalized Valence Bond Studies of Cu, Ag, Au, Li, and Na. *J. Phys. Chem.* **1988**, *92*, 1352–1365.

6 Glukhovtsev, M. N.; Schleyer, P. v. R. Polyatomic Molecules without Electron-Pair Bonds: High-Spin Trigonal, Tetrahedral and Octahedral Lithium Clusters. *Isr. J. Chem.* **1993**, *33*, 455–466.

7 (a) For reviews, see: Higgins, J.; Callegari, C.; Reho, J.; Stienkemeier, F.; Ernst, W. E.; Lehmann, K. K.; Gutowski, M.; Scoles, G. Photoinduced Chemical Dynamics of High-Spin Alkali Trimers. *Science* **1996**, *273*, 629–631. Higgins, J.; Callegari, C.; Reho, J.; Stienkemeier, F.; Ernst, W. E.; Gutowski, M.; Scoles, G. Helium Cluster Isolation Spectroscopy of Alkali Dimers in the Triplet Manifold. *J. Phys. Chem. A* **1998**, *102*, 4952–4965. (b) Brühl, F. R.; Miron, R. A.; Ernst, W. E. Triplet States of Rubidium Dimers on Helium Nanodroplets. *J. Chem. Phys.* **2001**, *115*, 10275–10281. (c) Higgins, J.; Hollebeck, T.; Reho, J.; Ho, T.-S.; Lehmann, K. K.; Rabitz, H.; Scoles, G.; Gutowski, M. On the Importance of Exchange Effects in Three-Body Interactions: The Lowest Quartet State of Na_3. *J. Chem. Phys.* **2000**, *112*, 5751–5761. Higgins, J.; Ernst, W. E.; Callegari, C.; Reho, J.; Lehmann, K. K.; Scoles, G. Spin Polarized Alkali Clusters: Observation of Quartet States of the Sodium Trimer. *Phys. Rev. Lett.* **1996**, *77*, 4532–4535. Reho, J.; Higgins, J.; Nooijen, M.; Lehmann, K. K.; Scoles, G.; M. Gutowski, M. Photoinduced Nonadiabatic dynamics in Quartet Na_3 and K_3 Formed Using Helium Nanodroplet Isolation. *J. Chem. Phys.* **2001**, *115*, 10265–10274. (d) Fioretti, A.; Comparat, D.; Crubellier, A.; Dulieu, O.; Masnou-Seeuws, F.; Pillet, P. Formation of Cold Cs_2 Molecules Through Photoassociation. *Phys. Rev. Lett.* **1998**, *80*, 4402–4405.

8 Bondybey, V. E. The Lowest a $^3\Sigma_u^+$ State of Cu_2. *J. Chem. Phys.* **1982**, *77*, 3771–3772.

9 (a) Dobson, J. Magnetic Micro- and Nano-Particle-Based Targeting for Drug and Gene Delivery. *Nanomedicine* **2006**, *1*, 31–37. Moroz, P.; Jones, S. K.; Gray, B. N. Magnetically Mediated Hyperthermia: Current Status and Future Directions. *Int. J. Hyperthermia* **2002**, *18*, 267–284. (b) Jung, H.; Kim, J.-W.; Choi, H.; Lee, J.-H.; Hur, H.-G. Synthesis of Nanosized Biogenic Magnetite and Comparison of its Catalytic Activity in Ozonation. *Appl. Catal. B: Environ after Environ.* **2008**, *83*, 208–213. (c) Periero, M.; Baldomir, D.; Arias, J. E. Unexpected Magnetism of Small Silver Clusters. *Phys. Rev. A* **2007**, *75*, No. 063204.

10 Naaman, R.; Vager, Z. New electronic and Magnetic Properties Emerging from Adsorption of Organized Organic Layers. *Phys. Chem. Chem. Phys.* **2006**, *8*, 2217–2224.

11 Tai, T. B.; Nhat, P. V.; Nguyen, M. T.; Li, S.; Dixon, D. A. Electronic Structure and Thermochemical Properties of Small Neutral and Cationic Lithium Clusters and Boron-Doped Lithium Clusters: $Li_n^{0/+}$ and $Li_nB^{0/+}$ (n = 1−8). *J. Phys. Chem. A* **2011**, *115*, 7673–7686.

12 (a) Monari, A.; Pitrach-Ruiz, J.; Endazzoli, G.-L.; Evangelisti, S.; Sanchez-Martin, J. Full-Configuration Interaction Study on the Tetrahedral Li_4 Cluster. *J. Chem. Theory Comput.* **2008**, *4*, 404–413. (b) Verdicchio, M.; Evangelisti, S.; Leininger, T.; Sanchez-Martin, J.; Monari, A. Coupled-Cluster Study of 'No-Pair' Bonding in the Tetrahedral Cu_4 Cluster. *Chem. Phys. Lett.* **2011**, *503*, 215–219.

13 Schreiner, P.; Chernish, L. V.; Gunchenko, P. A.; Tikhonchuk, E. Y.; Hausmann, H.; Serafin, M.; Schlecht, S.; Dahl, J. E. P.; Carlson, R. M. K.; Fokin, A. A. Overcoming Liability of Extremely Long Alkane Carbon−Carbon Bonds Through Dispersion Forces. *Nature* **2011**, *477*, 308–311.

14 Soldán, P.; Cvitas, M. T.; Huston, J. M. Three Body Nonadditive Forces between Spin-Polarizes Alkali-Metal Atoms. *Phys. Rev. A* **2003**, *67*, No. 054702.

15 (a) Wu, W.; Su, P.; Shaik, S.; Hiberty, P. C. Classical Valence Bond Approach by Modern Methods. *Chem. Rev.* **2011**, *111*, 7557–7593. (b) Braida, B.; Hiberty, P. C. The Essential Role of Charge-Shift Bonding in Hypervalent Prototype XeF_2. *Nat. Chem.* **2013**, *5*, 417–422.

16 Hiberty, P. C.; Humbel, S.; Archirel, P. Nature of the Differential Electron Correlation in Three-Electron Bond Dissociation. Efficiency of a Simple Two-Configuration Valence Bond Method with Breathing Orbitals. *J. Phys. Chem.* **1994**, *98*, 11697–11704. Hiberty, P. C. Reconciling Simplicity and Accuracy: Compact Valence Bond Wave Functions with Breathing Orbitals. *J. Mol. Struct. (Theochem)* **1997**, *398−399*, 35–43.

17 Goddard, W. A., III; Dunning, T. H.; Hunt, W. J.; Hay, P. J. Generalized Valence Bond Description of Bonding in Low-Lying States of Molecules. *Acc. Chem. Res.* **1973**, *6*, 368–376.

18 Pyykkö, P.; Desclaux, J.-P. Relativity and the Periodic System of Elements. *Acc. Chem. Res.* **1979**, *12*, 276–281.

19 Zayit, A.; Pinsky, M.; Elgavi, H.; Dryzun, C.; Avnir, D. A website for calculating the degree of chirality. *Chirality* **2011**, *23*, 17–23. Elgavi, H.; Krekeler, C.; Berger, R.; Avnir, D. Chirality in Copper Nanoalloy Clusters. *J. Phys. Chem. C* **2012**, *116*, 330–335.

20 For ELF, see: Silvi, A.; Savin, A. Classification of Chemical Bonds Based on Topological Analysis of Electron Localization Functions. *Nature* **1994**, *371*, 683–686.

21 Alikhani, M. E.; Shaik, S. A Topological Study of the Ferromagnetic "No-Pair Bonding" in Maximum-Spin Lithium Clusters: $^{n+1}Li_n$ (n=2−6). *Theor. Chem. Acc.* **2006**, *116*, 490–397.

22 For a recent Mg-Mg bonded molecule, see: Green, S. P.; Jones, C.; Stasch, A. Stable Magnesium(I) Compounds with Mg-Mg Bonds. *Science* **2007**, *318*, 1754–1757.

23 See a recent discussion: Neese, F.; Pantazis, D. A. What is Not Required to Make a Single Molecule Magnet. *Faraday Discuss.* **2011**, *148*, 229–238.

24 For a discussion of these issues in a Fermi gas of ^6Li with ^7Li bosons, see: Cvitas, M. T.; Soldán, P.; Houston, J. M.; Honvault, P.; Launay, J.-M. Ultracold Collisions Involving Heteronuclear Alkali Metal Dimers. *Phys. Rev. Lett.* **2005**, *94*, No. 200402.

25 Lange, K. K.; Tellgren, E. I.; Hoffmann, M. R.; Helgaker, T. A Paramagnetic Bonding Mechanism for Diatomics in Strong Magnetic Fields. *Science* **2012**, *337*, 327–331. Schmelcher, P. Molecule Formation in Ultrahigh Magnetic Fields. *Science* **2012**, *337*, 302–303.

26 See also: Schmelcher, P.; Cederbaum, L. S. Molecules in Strong Magnetic Fields: Properties of Atomic Orbitals. *Phys. Rev. A* **1988**, *37*, 672–681.